

Dynamical phase shift in x-ray absorption and ionization spectra by two delayed x-ray laser fieldsViktoriia Savchenko ^{1,2}, Faris Gel'mukhanov,^{1,2,3} Tim Laarmann ^{4,5}, Sergey P. Polyutov ^{1,6}, and Victor Kimberg ^{1,2,*}¹*International Research Center of Spectroscopy and Quantum Chemistry—IRC SQC, Siberian Federal University, 660041 Krasnoyarsk, Russia*²*Department of Theoretical Chemistry and Biology, KTH Royal Institute of Technology, 10691 Stockholm, Sweden*³*Institute for Methods and Instrumentation in Synchrotron Radiation Research FG-ISRR, Helmholtz-Zentrum Berlin für Materialien und Energie, Albert-Einstein-Strasse 15, 12489 Berlin, Germany*⁴*Deutsches Elektronen-Synchrotron DESY, Notkestr. 85, 22607 Hamburg, Germany*⁵*The Hamburg Centre for Ultrafast Imaging CUI, Luruper Chaussee 149, 22761 Hamburg, Germany*⁶*Kirensky Institute of Physics, Federal Research Center KSC SB RAS, 660036 Krasnoyarsk, Russia*

(Received 24 March 2021; revised 4 May 2021; accepted 2 July 2021; published 26 July 2021)

We study theoretically x-ray absorption and ionization spectra of an atom or molecule by two coherent x-ray pulses that show a relative phase shift resulting in a time delay of the pulse envelopes. We demonstrate that the phase modulation of the spectra is shifted with respect to the phase oscillation comb of the x-ray double pulse. The reason for this shift is the dynamics of the process defined by the interplay of the delay time, the pulse width, the detuning, and the lifetime of the core-excited state.

DOI: [10.1103/PhysRevA.104.013114](https://doi.org/10.1103/PhysRevA.104.013114)**I. INTRODUCTION**

Coherent steering of a quantum system by light enabling manipulation by populations and interfering pathways is one of the attractive areas of study in optical physics [1–5] and photochemistry [3]. Due to the fast development of laser technology in the x-ray spectral range this research area is moving rapidly into the short-wavelength region [6–10]. The shaping of the laser phases and their coherence becomes the central concept to control quantum interference x-ray phenomena [11,12]. The modern synchrotron [7], x-ray free-electron laser, or high-harmonic generation light sources [12–14] allow one to use temporally overlapping, mutually coherent wavelengths; a single wave packet split into temporally separated pulses with controlled relative phase; or other optical arrangements. Usually, the role of the phase is studied in the case of a polychromatic short-wavelength field. Good examples of such kind of phenomena are interference of one- and two-photon ionization channels controlled by the phase shift [8,12] and the coherent control of the population of the Rydberg states by the time delay of the light wave packet pair with the broad spectral bandwidth [7]. However, there is a possibility of a mismatch of the phase of the linear x-ray response and the phase of the driving weak close to monochromatic x-ray laser field composed from two time-delayed short coherent x-ray pulses. Recent experiments [10]

revealed such a phase shift of the x-ray response relative to the phase of the incoming coherent pulse replicas for Auger decay accompanied by shake-up excitation, while no shift was observed for the x-ray photoelectron spectroscopy (XPS) and participator Auger processes. This behavior was assigned to the correlated electronic dynamics.

The natural question that arises, however, is with regard to the only possible reason for the observed phase shift: is this shift related solely to the microscopic peculiarities of the studied system like interelectron correlation [10] or can it also be triggered by general dynamic effects of the interaction of two coherent phase-shifted x-ray pulses with the quantum system? To shed light on the problem we study here a simple situation of the x-ray absorption spectrum (XAS) for a two-level quantum system. In many atomic and molecular systems, the lowest core-excited state is well separated by a few electron volts from the higher core-excited states, which are significantly larger as compared to the $\lesssim 1$ -eV spectral bandwidth of a typical few-femtosecond-duration x-ray pulse. This makes our results applicable to a large class of systems under core excitation. To make the picture complete, the case of a few close-lying core-excited states is also discussed in the present contribution. We show that at increased delay time between the pulse replicas the main reason for the phase shift becomes the interaction dynamics. More precisely, the absorption of the two phase-shifted and time-delayed x-ray fields consists of two coherent absorption channels. Apparently the relative phase dependence appears from interference of these channels. We show that the interference term in the XAS, defined by dynamical overlap of time-delayed coherent pulses, brings an extra phase shift. The discussed phenomena and presented theory are also applied for the XPS. The results are obtained for the atomic targets, since no vibrational dynamics is included; however, our conclusions can be also applied for simple molecules. In molecules, the situation will be more

*kimberg@kth.se

Published by the American Physical Society under the terms of the [Creative Commons Attribution 4.0 International](https://creativecommons.org/licenses/by/4.0/) license. Further distribution of this work must maintain attribution to the author(s) and the published article's title, journal citation, and DOI. Funded by [Bibsam](https://www.bibsam.com/).

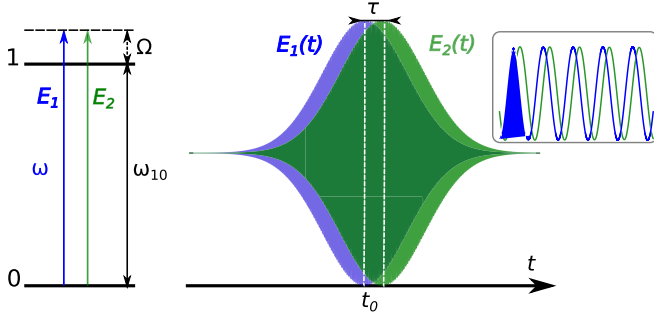


FIG. 1. Scheme of transitions and temporal alignment of the two delayed coherent x-ray pulses.

complex due to vibrational and rotational degrees of freedom, yet the discussed dynamics phase shift will be present.

The paper is organized as follows. In Sec. II our theoretical framework is presented. The results of simulations and their discussions are given in Sec. III. The main conclusions of the paper are summarized in Sec. IV.

II. THEORY

A. General description of the interaction with two delayed x-ray pulses

Let us consider the interaction of a two-level atomic or molecular system with two time-delayed (phase-shifted) coherent x-ray pulses of the same frequency ω (Fig. 1):

$$\begin{aligned} \mathcal{E}(\omega, t) &= \frac{1}{2} \mathbf{E}(t) e^{i\omega t} + \text{c.c.}, \quad \mathbf{E}(t) = \mathbf{e} E(t), \\ E(t) &= E_1(t) + E_2(t) e^{i\varphi}, \quad E_n(t) = E_n^0 \Phi_n(t). \end{aligned} \quad (1)$$

Here \mathbf{e} is the polarization vector of the x-ray field \mathcal{E} , E_n^0 is the maximal value of the pulse envelope $E_n(t)$, and $\Phi_n(t)$ is the temporal profile of each component ($n = 1$ and 2). The phase shift $\varphi = \phi - \omega\tau$ depends on the absolute phase shift ϕ between the fields and the temporal delay τ between the pulses [12]. The interference of these coherent x-ray fields results in the field intensity given by

$$I(t) \propto |E(t)|^2 \equiv |E_1(t)|^2 + |E_2(t)|^2 + 2E_1(t)E_2(t) \cos \varphi, \quad (2)$$

which experiences oscillations with variation of the phase. We intend to understand the relationship between the phase shift of x-ray absorption and φ .

Let us calculate the absorption probability from the ground ψ_0 to the core-excited ψ_1 states. The total wave function of the system in the interaction picture $\psi = a_1 \psi_1 + a_0 \psi_0$ is the coherent superposition of states ψ_0 and ψ_1 . Neglecting the depopulation of the ground state by the weak x-ray pulses, the amplitudes a_0 and a_1 satisfy the following equations in the rotating-wave approximation (in atomic units):

$$\dot{a}_1 + \Gamma a_1 = i G_{10}(t) e^{-i\Omega t}, \quad a_0 \approx 1, \quad (3)$$

where $\Omega = \omega - \omega_{10}$ is the detuning from the absorption resonance, ω_{10} is the resonant frequency of core excitation with the transition dipole moment \mathbf{d}_{10} between core-excited and ground states, and Γ is the lifetime broadening (half width at half maximum, HWHM). In Eq. (3) and below, we use

the weak-field approximation, which is valid for the range of x-ray pulse intensities used in the correspondent experiments ($\lesssim 10^{15}$ W/cm² [10]) due to the rather small value of the transition dipole moment of the core excitation and short pulse duration (for more details, see Sec. III). The time dependence of the Rabi frequency $G_{10}(t) = [\mathbf{E}(t) \cdot \mathbf{d}_{10}]/2$ is defined by the envelope of the x-ray laser field $E(t)$. The solution of the amplitude Eqs. (3) is straightforward:

$$a_1(t) = i e^{-\Gamma t} \int_0^t G_{10}(t_1) e^{-i(\Omega+i\Gamma)t_1} dt_1. \quad (4)$$

In the present model the off-diagonal element of the density matrix $\rho_{10}(t) = a_1(t) a_0^*(t) \approx a_1(t)$, and the equation for the instantaneous value of the absorption probability reads as follows:

$$\begin{aligned} \sigma_{\text{inst}}(\omega, t) &= 2\text{Im}[\rho_{10}(t) G_{01}(t) e^{i\Omega t}] \\ &= 2\text{Re} \left(G_{01}(t) e^{i\Omega t} e^{-\Gamma t} \int_{t_{\min}}^t G_{10}(t_1) e^{-i\Omega t_1} e^{\Gamma t_1} dt_1 \right). \end{aligned} \quad (5)$$

This equation directly shows that the phase dependence of the absorption copies exactly the one of the intensity (2) in the case of continuum-wave x rays or long pulses, because $G_{01}(t) G_{10}(t) = |G_{01}(t)|^2 \propto |E_1(t)|^2 + |E_2(t)|^2 + 2E_1(t)E_2(t) \cos \varphi$. Let us now apply the experimental double-pulse situation where the x-ray absorption probability (5) is integrated over time, corresponding to the acquisition time or the readout time of the photosensitive device, which is usually much longer as compared to the duration of x-ray pulses. The integrated absorption cross section reads as follows:

$$\begin{aligned} \sigma(\omega) &= \zeta \text{Re} \left(\int_{t_{\min}}^{t_{\max}} dt G_{01}(t) e^{i\Omega t} e^{-\Gamma t} \int_{t_{\min}}^t G_{10}(t_1) e^{-i(\Omega+i\Gamma)t_1} dt_1 \right). \end{aligned} \quad (6)$$

Here we extracted the polarization factor $\zeta = \overline{|\mathbf{e} \cdot \mathbf{d}_{10}/d_{10}|^2}$, where the overline means orientations averaging, so that $G_{10}(t) = E(t) d_{10}/2$ is a product of scalars. The bounds of integration t_{\min} and t_{\max} can be chosen reasonably accounting for the x-ray pulse envelopes $\Phi_1(t)$ and $\Phi_2(t)$, as discussed below. The Rabi frequency for phase-shifted, i.e., time-delayed, two x-ray pulses reads

$$\begin{aligned} G_{10}(t) &= G_{01}^*(t) = G[g_1 \Phi_1(t) + g_2 \Phi_2(t) e^{i\varphi}], \\ g_n &= \frac{E_n^0}{\sqrt{(E_1^0)^2 + (E_2^0)^2}}, \\ \Phi_1(t) &= \exp \left[-\frac{1}{2} \left(\frac{t-t_0}{T} \right)^{2k} \ln 2 \right], \\ \Phi_2(t) &= \exp \left[-\frac{1}{2} \left(\frac{t-t_0-\tau}{T} \right)^{2k} \ln 2 \right], \end{aligned} \quad (7)$$

where $G = \sqrt{(E_1^0)^2 + (E_2^0)^2} \times d_{10}/2$ and t_0 is the position of the maximum of the first pulse envelope $\Phi_1(t)$. The present form of the envelope shape used in our simulations describes

a smooth transition from Gaussian ($k = 1$) to rectangular ($k \gg 1$) pulse. If the shape of the pulse is close to rectangular one can already start in the simulation from $k = 3$ [6]. Here τ is the time delay of the second pulse relative to the first one and T is the half width at half maximum of the pulse intensity distribution in the time domain, i.e., a measure of the x-ray pulse duration.

As it can be seen from Eqs. (6) and (7), the phase dependence of the XAS reflects the phase dependence of the x-ray field when the pulses are much longer than the lifetime of the core-excited state $1/\Gamma$ and the delay time τ (for example, continuum wave x-ray light),

$$\sigma(\omega, \tau) \propto |g_1 + g_2 e^{i\varphi}|^2 = g_1^2 + g_2^2 + 2g_1g_2 \cos \varphi, \quad (8)$$

or in a trivial case, when the two pulses are overlapped $\tau = 0$, $\Phi_1(t) = \Phi_2(t) = \Phi(t)$, and $\varphi = \phi$. Otherwise, one should expect the deviation of the phase dependence of $\sigma(\omega, \tau)$ from the x-ray field dependence. Let us illustrate this with a simple case allowing for an analytical description.

B. Analytical solution for a cos-pulse shape

1. X-ray absorption spectra

Let us first analyze a simple model for a XAS using the x-ray pulse envelope that allows one to get analytical results and thus to understand the main physical picture of the phenomena. This can be done using the cos-envelope model for the x-ray fields:

$$\begin{aligned} \Phi_1(t) &= \cos\left(\frac{\pi t}{4T}\right) f_1(t), & \Phi_2(t) &= \cos\left(\frac{\pi(t-\tau)}{4T}\right) f_2(t), \\ f_1(t) &= 1, & \text{when } -T \leq t \leq T, \\ f_2(t) &= 1, & \text{when } \tau - T \leq t \leq \tau + T, \end{aligned} \quad (9)$$

and $f_1(t) = f_2(t) = 0$ otherwise. The intensity pulse HWHM T is here equivalent to the one defined for a Gaussian function (7). Integration of Eq. (6) with the pulse shape (9) in the limit of $\tau \ll T$ and $T\Gamma, T|\Omega| \ll 1$ allows one to get an analytical expression for the phase-dependent contribution to the XAS cross section:

$$\begin{aligned} \sigma(\omega, \tau) &= \sigma_0(\omega, \tau) + \sigma_\varphi(\omega, \tau), \\ \sigma_\varphi(\omega, \tau) &\approx |G|^2 \frac{g_1 g_2}{3} \left(\frac{4T\Gamma}{\Omega^2 + \Gamma^2} \right) \cos[\varphi + \delta(\omega, \tau)], \end{aligned} \quad (10)$$

$$\sigma(\omega, \tau) = \sum_n \sigma_n(\omega, \tau),$$

$$\sigma_n(\omega, \tau) = \zeta_n \text{Re} \left(\int_{t_{\min}}^{t_{\max}} dt G_{0n}(t) e^{i\Omega_n t} e^{-\Gamma t} \int_{t_{\min}}^t G_{n0}(t_1) e^{-i(\Omega_n + i\Gamma)t_1} dt_1 \right). \quad (14)$$

As one can see from Eq. (11), each n th core-excited state has its own dynamical phase shift δ_n due to the difference in the spectral detuning $\Omega_n = \omega - \omega_{n0}$. Since the close-lying resonances usually overlap, the total dynamical phase shift

with the additional phase shift

$$\delta(\omega, \tau) \approx \frac{2\pi \Omega \sin(\pi \tau / 2T)}{T(\Omega^2 + \Gamma^2)} \quad (11)$$

in the XAS profile $\cos(\varphi + \delta)$ with respect to the x-ray intensity dependence $\cos \varphi$. The dynamical phase shift δ vanishes when $\tau = 0$ or $\Omega = 0$ and tends to zero as $1/T^2$ with increasing pulse duration. The phase-independent part of the cross section $\sigma_0(\omega, \tau)$ is defined in Sec. II C.

2. X-ray core ionization

Let us now consider the x-ray ionization of the core level of an atom by the monochromatic x-ray field (1) with the frequency ω . The XPS process, where a photoelectron with kinetic energy ϵ is detected [15], can be described by the same equations as the XAS; however, now the total energy of the final state equals to $\epsilon + E^+$, where E^+ is the energy of the core-ionized atom. Therefore, the detuning in Eqs. (3) and (11) reads $\Omega = \omega - (\epsilon + E^+ - E_0) = \omega - I - \epsilon$, where I is the ionization potential of the core level. Thus the dynamical phase (11) for the XPS reads

$$\delta(\omega, \tau) \approx -\frac{2\pi (\epsilon - \epsilon_{\text{res}}) \sin(\pi \tau / 2T)}{T[(\epsilon - \epsilon_{\text{res}})^2 + \Gamma^2]}, \quad \epsilon_{\text{res}} = \omega - I. \quad (12)$$

We see below that the dynamical phase shift is small, $|\delta| \ll |\varphi|$, which allows us to use the Taylor expansion of the cross section (10):

$$\sigma_\varphi(\omega, \tau) \approx |G|^2 \frac{g_1 g_2}{3} \left(\frac{4T\Gamma}{(\epsilon - \epsilon_{\text{res}})^2 + \Gamma^2} \right) (\cos \varphi - \delta \sin \varphi). \quad (13)$$

In Ref. [10] the photoelectrons within a 5-eV energy interval around the resonant kinetic energy ϵ_{res} were collected, which means that the cross section (13) and, hence, the phase shift δ should be averaged over ϵ . This results in a zero dynamical phase shift $\bar{\delta} = 0$ for the XPS in full agreement with the measurements of the L ionization of the Ar atom [10].

3. Multilevel system

The obtained solution for the two-level system (11) allows one to understand what one can expect in the case of few close-lying core-excited states. For example, this is the case of a molecular system with close-lying vibrational levels ϵ_n of a core-excited electronic state. In this case the cross section (6) is the sum of the partial core-excitation cross sections $\sigma_n(\omega, \tau)$:

for a multilevel system is defined by the transition dipole moments for the n th state d_{n0} (or Franck-Condon factors for vibrational levels) and the detuning. This makes the effect rather complicated and requires thorough consideration for

each particular system. For example, the effect can be canceled by the contributions from the states with positive and negative detuning (11). In the present study we focus on details of the dynamical phase shift for the two-level system, which is a quite abundant case in atomic spectroscopy.

C. Numerical simulations

In our simulations we use strict numerical integration of Eq. (6) with generalized Gaussian pulse envelopes (7). Before embarking on the detailed calculations, we rewrite Eq. (6) in terms of real functions, which are better suited for numerical

simulations. As it was shown above, the total XAS profile can be presented as a sum of two contributions:

$$\begin{aligned}\sigma(\omega, \tau) &= \sigma_0(\omega, \tau) + \sigma_C(\omega, \tau) \cos(\varphi) + \sigma_S(\omega, \tau) \sin(\varphi) \\ &= \sigma_0(\omega, \tau) + \sigma_\varphi(\omega, \tau) \cos(\varphi + \delta), \\ \sigma_\varphi(\omega, \tau) &= \eta \sqrt{[\sigma_C(\omega)]^2 + [\sigma_S(\omega)]^2}, \quad \eta = \text{sgn}[\sigma_C(\omega)], \\ \delta(\omega, \tau) &= -\arctan\left(\frac{\sigma_S(\omega, \tau)}{\sigma_C(\omega, \tau)}\right),\end{aligned}\quad (15)$$

where the partial cross sections are defined as follows:

$$\begin{aligned}\sigma_0(\omega, \tau) &= G^2 \zeta \int_{t_{\min}}^{t_{\max}} dt_1 \left[Q_1^C(t) F_1^C(t) + Q_1^S(t) F_1^S(t) + Q_2^C(t) F_2^C(t) + Q_2^S(t) F_2^S(t) \right], \\ \sigma_C(\omega, \tau) &= G^2 \zeta \int_{t_{\min}}^{t_{\max}} dt_1 \left[Q_1^C(t) F_2^C(t) + Q_2^C(t) F_1^C(t) + Q_1^S(t) F_2^S(t) + Q_2^S(t) F_1^S(t) \right], \\ \sigma_S(\omega, \tau) &= G^2 \zeta \int_{t_{\min}}^{t_{\max}} dt_1 \left[Q_1^S(t) F_2^C(t) + Q_2^C(t) F_1^S(t) - Q_1^C(t) F_2^S(t) - Q_2^S(t) F_1^C(t) \right].\end{aligned}\quad (16)$$

The intermediate real functions we operated in our simulations,

$$\begin{aligned}Q_n^C(t) &= g_n \Phi_n(t) \cos(\Omega t) e^{-\Gamma t}, \quad Q_n^S(t) = g_n \Phi_n(t) \sin(\Omega t) e^{-\Gamma t}, \\ F_n^C(t) &= g_n \int_{t_{\min}}^t dt_1 \Phi_n(t_1) \cos(\Omega t_1) e^{\Gamma t_1}, \quad F_n^S(t) = g_n \int_{t_{\min}}^t dt_1 \Phi_n(t_1) \sin(\Omega t_1) e^{\Gamma t_1},\end{aligned}\quad (17)$$

have qualitatively different dependence on the detuning from the absorption resonance Ω . Indeed, $Q_n^C(t)$ and $F_n^C(t)$ are even functions, while $Q_n^S(t)$ and $F_n^S(t)$ are odd functions of Ω . Moreover $Q_n^S(t) = F_n^S(t) = 0$ when $\Omega = 0$. Due to this, we can conclude, that when the photon frequency approaches strict XAS resonance, the phase shift vanishes, since $\sigma_S = 0$ for $\Omega = 0$. Furthermore, for the case of a single pulse ($\tau = 0$), when $Q_1^{S,C} \equiv Q_2^{S,C}$ and $F_1^{S,C} \equiv F_2^{S,C}$, the dynamic phase shift $\delta = 0$ also disappears ($\sigma_S = 0$). Similar behavior has already been illustrated for the analytical solution (11).

III. RESULTS AND DISCUSSIONS

Here we study the interaction of the two coherent and temporally (phase) shifted x-ray pulses with a model two-level quantum system, as it is schematically depicted in Fig. 1. Level 0 represents the ground state of the system, and level 1 correspond to the core-hole state (core-excited or core-ionized state). Our simulations are adapted for a typical two-level situation of the *K*- or *L*-edge excitation in the soft x-ray spectral range, e.g., $2p_{1/2} \rightarrow 4s$ ($\omega_{10} = 246.5$ eV) or $2p_{3/2} \rightarrow 4s$ ($\omega_{10} = 244.3$ eV) XAS *L* transitions in argon atom with $\Gamma = 0.056$ eV [16]. The two-level approximation is also valid for the C *K*-edge $X^1\Sigma^+ \rightarrow C 1s^{-1}2\pi^1$ transition in CO, which is free from vibrational broadening [17]. In what follows, we suppose $\phi = 0$, which is the case in typical experiments with coherent pulses generated by a beam splitter providing collinear propagation of both pulse replicas and thus constant phase difference across the beam profile [18,19]. However, the presence of a constant value of ϕ would not affect the general discussion presented below. We follow typically avail-

able experimental parameters [10] for x-ray pulses with $T = 0.5, \dots, 5$ fs and $\tau = 0, \dots, 0.5$ fs. We suppose equal intensity for both x-ray pulses $g_1 = g_2 = 1/\sqrt{2}$ and analyze the dependence on the double-pulse envelope for Gaussian ($k = 1$) and rectangular ($k = 3$) pulses.

Moreover, we choose an arbitrary weak intensity of the x-ray field, which does not change the population $G^2 \ll 1$, and compute all partial cross sections in arbitrary units (all cross sections (16) have the same prefactor $G^2 \zeta$). Let us show that the chosen weak-field assumption is valid for typical experimental conditions. Following the recent experiment at the FLASH facility [10] we base our analysis on the *L*-edge absorption of argon and use an x-ray pulse intensity of about 10^{15} W/cm² and a pulse duration of a few femtoseconds. Using the value of the transition dipole moment $d_{10} \approx 0.02$ a.u., we get the Rabi frequency $G_{10} \approx (14 \text{ fs})^{-1}$. The population of the core-excited state is given by the ‘‘area of the pulse’’ according to the Rabi solution: [4,16]

$$\begin{aligned}\rho_{11}(t) &= |a_1(t)|^2 = \sin^2 \theta(t), \\ \theta(t) &= \int_{-\infty}^t G_{10}(t) dt \sim G_{10} T.\end{aligned}$$

For the pulse duration $T = 2$ fs we get $\theta \approx 0.14 \ll 1$ and hence $\rho_{11} \approx \theta^2 \approx 0.02 \ll 1$. This means that we are essentially in the linear regime and the role of nonlinear effects is weak.

Let us start with the analysis of the XAS spectral profile, shown in Fig. 2, where the two terms of Eq. (16) are separated: panels (a) and (b) represent σ_0 , while panels (c) and (d) show the phase-shifted contribution $\sigma_\varphi \cos(\varphi + \delta)$.

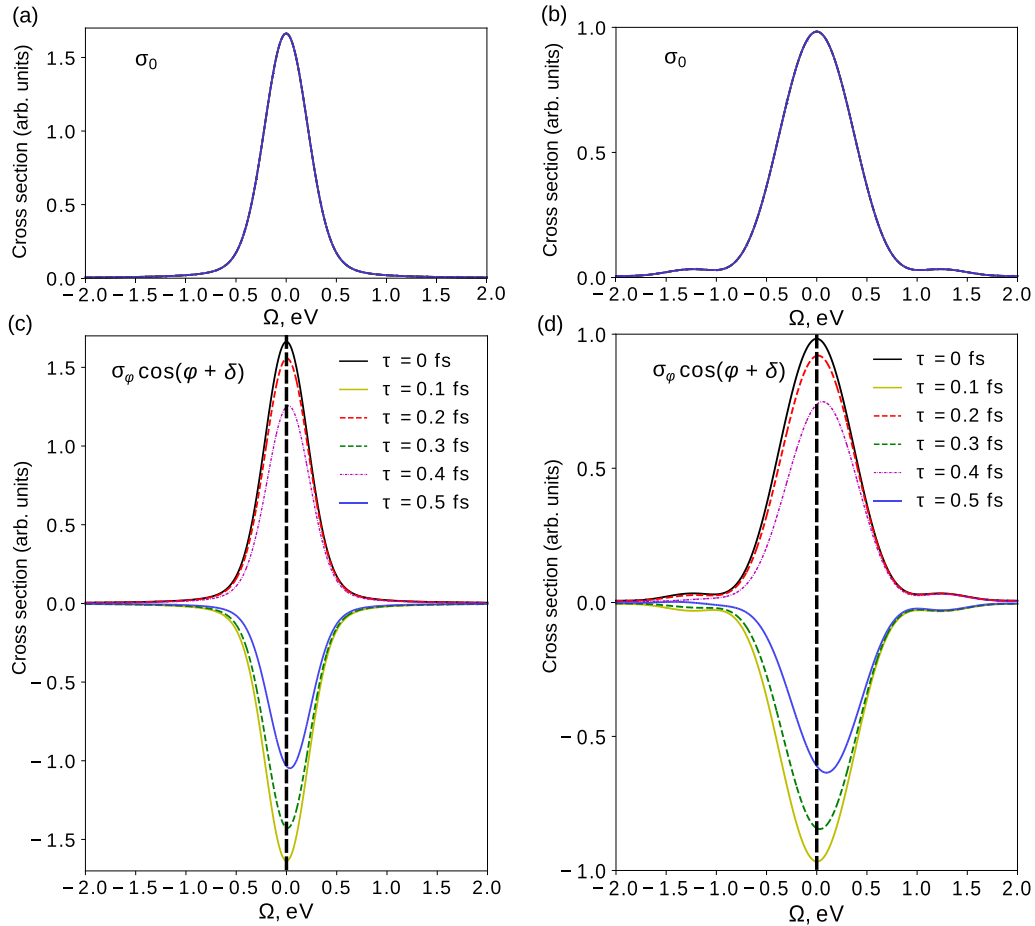


FIG. 2. XAS cross section $\sigma(\omega, \tau)$, Eq. (15), as a function of detuning Ω from resonance for $T = 2$ fs and various values of τ (see legends). The cases of Gaussian pulse shapes $k = 1$ (a, c) and rectangular pulses $k = 3$ (b, d) are compared. The phase-independent cross section $\sigma_0(\omega, \tau)$ does not display the dependence on the time delay τ in the studied range of parameters for both Gaussian (a) and rectangular (b) pulses contrary to $\sigma_\varphi(\omega, \tau) \cos(\varphi + \delta)$, which shows strong τ dependence.

Here we compare the Gaussian, panels (a) and (c), and the rectangular, panels (b) and (d), pulse shapes. The shape of σ_0 apparently does not depend on the delay time τ between the two pulses; however, the spectral shape is modified in the case of rectangular pulses forming some low-intensity side bands near $\Omega = \pm 1.2$ eV. This term, however, does not have much importance for our study, since this contribution can be easily extracted, when for example x-ray transient absorption spectra (XTAS) are measured by recording data at $\tau = 0$:

$$\begin{aligned} \sigma_{\text{XTAS}}(\omega, \tau) &= \sigma(\omega; \tau) - \sigma(\omega; 0) \\ &\approx \sigma_\varphi(\omega, 0)[\cos(\varphi + \delta) - 1], \end{aligned} \quad (18)$$

since $\sigma_\varphi(\omega; \tau)/\sigma_\varphi(\omega; 0) \approx 1$ for $\tau \lesssim 3$ fs, according to our simulations. The term $\sigma_\varphi(\omega; 0)$ is shown by the black line in Figs. 2(c) and 2(d) and reflects the shape of σ_0 . Let us now look in more detail for the dependence of the second term $\sigma_\varphi \cos(\varphi + \delta)$ on the variation of the delay time [Figs. 2(c) and 2(d)]. It is worthwhile noting that this term contains both the ordinary phase shift $\varphi(\omega, \tau)$ and the dynamic phase shift $\delta(\omega, \tau)$, which results in two qualitatively different features. The first gross feature is the modulation proportional to the ordinary phase shift $\sim \cos[\varphi(\omega, \tau)]$ expressed in a strong

change of the value and its sign with changing τ . The second and minor feature observed in some small shift of the XAS peak from position $\Omega = 0$ is related to the additional dynamic phase shift $\delta(\omega, \tau)$ (see also Figs. 3 and 4 and the text below). This effect is stronger for the rectangular pulse shape.

The observable $\sigma_{\text{XTAS}}(\omega, \tau) \propto \cos(\varphi + \delta) - 1$ given by Eq. (18) is presented in Fig. 3 as a function of delay time τ for three different intervals and three values of the detuning from resonance $\Omega = 0, 0.1, \text{ and } 0.5$ eV. The case of $\Omega = 0$ corresponds to the case when the dynamic shift is absent ($\delta = 0$). One can see that for the larger absolute values of the delay time the induced dynamic shift becomes stronger. It, however, is negligibly small at τ close to zero.

In order to understand this effect in more detail, let us focus now on the dependence of the dynamic phase shift δ on various parameters of the x-ray laser pulses (photon energy detuning, delay time, pulse duration, and pulse shape). The dependence on detuning is presented in Fig. 4 for variation of the delay time [panel (a)] and the pulse duration [panel (b)]. As it was already discussed from the analytical analysis, the dynamic phase shift is absent ($\delta = 0$) for zero values of the delay time and detuning, which is clearly seen

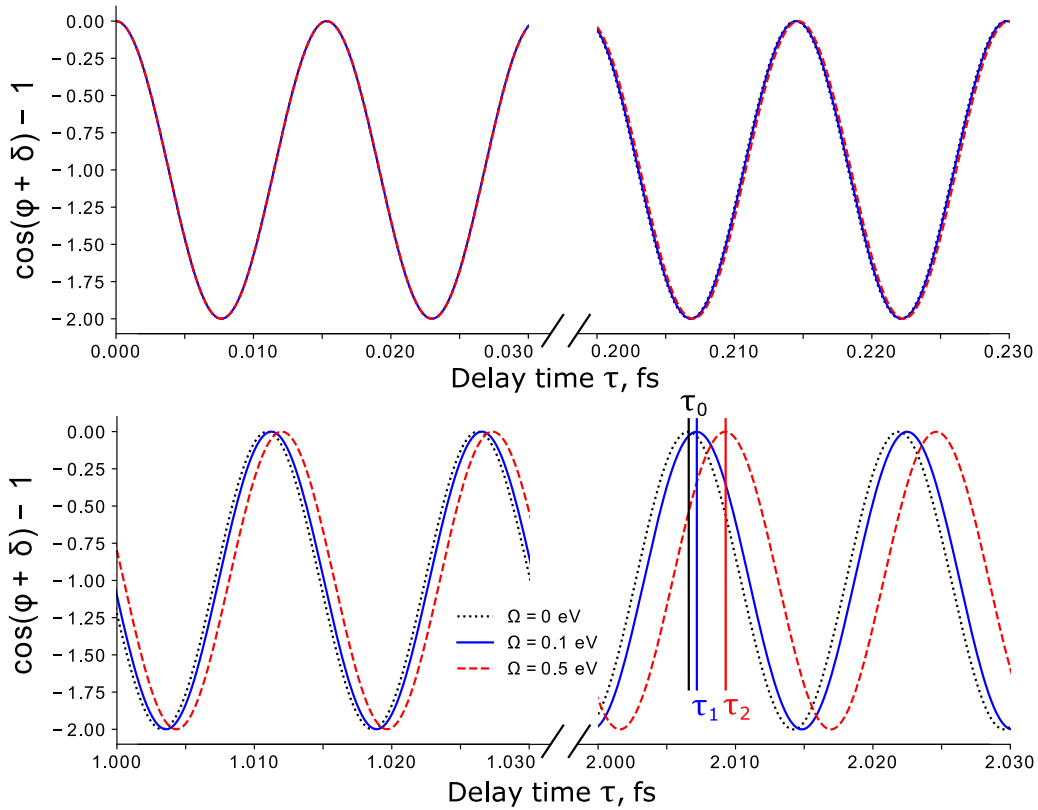


FIG. 3. XTAS observable $\sigma_{\text{XTAS}}(\omega, \tau)/\sigma_{\varphi}(\omega, \tau)$ according to Eq. (18) as a function of the delay time τ in three different intervals. The cases of $\Omega = 0, 0.1$, and 0.5 eV are presented by dotted, solid, and dashed lines, respectively. The maxima of the XTAS profile near $\tau = 2$ fs are marked by τ_0, τ_1 , and τ_2 for $\Omega = 0, 0.1$, and 0.5 eV, respectively. The dynamic phase shift near $\tau = 2$ fs results in a time delay of $\tau_2 - \tau_0 = 2.6$ as and $\tau_1 - \tau_0 = 0.6$ as for $\Omega = 0.1$ and 0.5 eV, respectively (the dynamic phase shift for $\Omega = 0$ is 0). $T = 2$ fs.

from the full numerical simulations. For the constant pulse duration $T = 2$ fs [Fig. 4(a)], the spectral dependence forms two antisymmetric peaks near $\Omega = \pm 0.5$ eV; the values of these peaks increase with increases of the delay time τ . The energy position of these features is shifting towards $\Omega = 0$ and its value decreases with increasing of the pulse duration T [Fig. 4(b)].

Figure 5 shows the dependence of δ on the delay time τ for the fixed pulse duration $T = 2$ fs and two values of detuning from resonance. $\Omega = 0.5$ eV corresponds to the position of the spectral feature [see Fig. 4(a)], thus showing

much stronger dependence, as compared to the case of $\Omega = 0.1$ eV. The dynamic phase shift δ as a function of τ experiences a periodic behavior with maximal value $\delta = \pi/2$ at $\tau \approx 3.5$ fs. Such a periodic behavior, however, can be hardly observed in the experiment for the delay time much larger than the pulse duration $\tau \gg T$, since for the nonoverlapping pulses $\sigma_C, \sigma_S \rightarrow 0$, as it follows from Eqs. (16) and (17), and the value of the term σ_{φ} in Eq. (15) becomes negligibly small. The x-ray pulse shape has also a clear effect here: the maximum value of $\delta = \pi/2$ is reached for the smaller delay time of $\tau \approx 2.5$ fs for rectangular pulses [Fig. 5(b)]

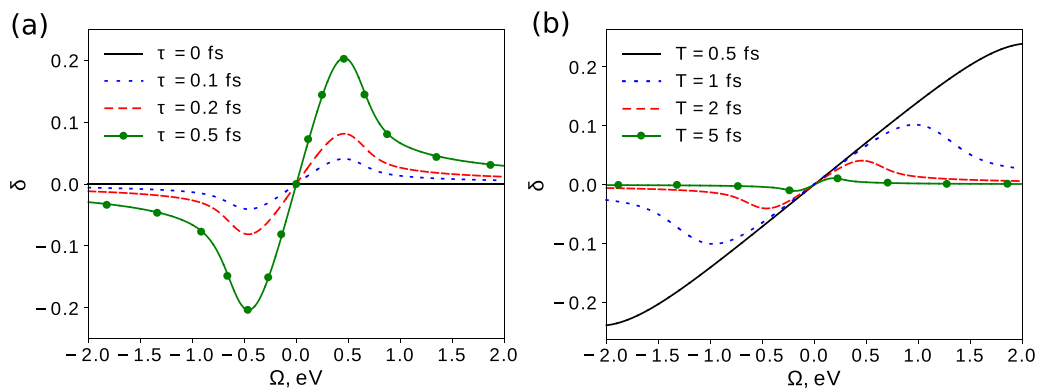


FIG. 4. The dynamics phase shift δ as a function of detuning Ω for Gaussian pulses $k = 1$. (a) $T = 2$ fs; $\tau = 0, 0.1, 0.2$, and 0.5 fs. (b) $\tau = 0.1$ fs; $T = 0.5, 1, 2$, and 5 fs.

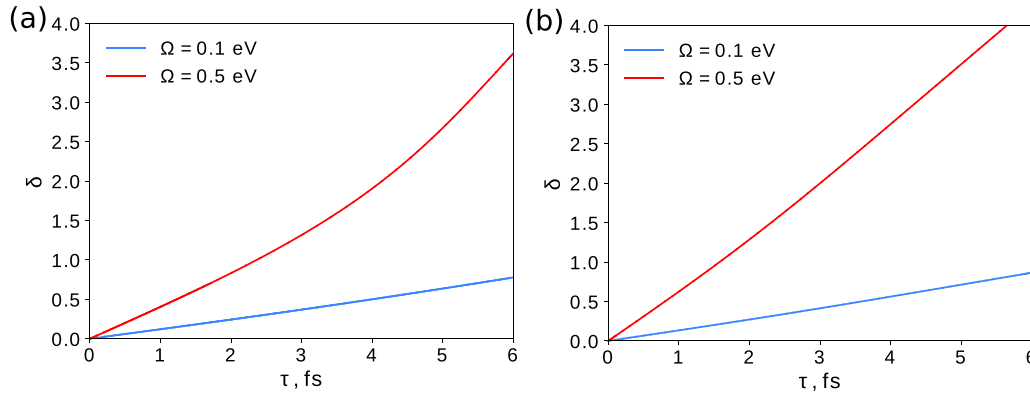


FIG. 5. The dynamics phase shift δ as a function of delay time $0 < \tau < 3T$ for fixed T and Ω describing transition from overlapping pulses to nonoverlapping pulses. $T = 2$ fs, $\Omega = 0.1$ and 0.5 eV, (a) $k = 1$, (b) $k = 3$.

compared to Gaussian envelopes. Moreover, for rectangular pulses, the sufficient overlap of the envelopes $\Phi_1(t)$ and $\Phi_2(t)$ is larger as compared to Gaussian pulses. These two factors makes rectangular pulses more favorable for the experimental observation of δ variation in a large range of delay times $\tau \leq T$.

Let us also compare the full theoretical simulation presented in Fig. 5 with an approximate analytical solution (11) described in Sec. II B. The results of the comparison are shown in Fig. 6, where an exact solution is presented in solid lines and the analytic approximation is given by dashed lines. Here we see qualitative agreement between the full theory and the approximation on the increase of the delay time τ , yet the approximation is overestimating the δ value. Let us note, however, that the formula (11) is derived in approximation $|T\Omega| \ll 1$, which is satisfied for $\Omega = 0.1$ eV and $T = 2$ fs ($|T\Omega| \approx 0.3$), but it is broken for $\Omega = 0.5$ ($|T\Omega| \approx 1.5$).

With the fixed delay time $\tau = 0.2$ fs the maximum absolute value of δ is reached for the shortest pulse duration $T \rightarrow 0$

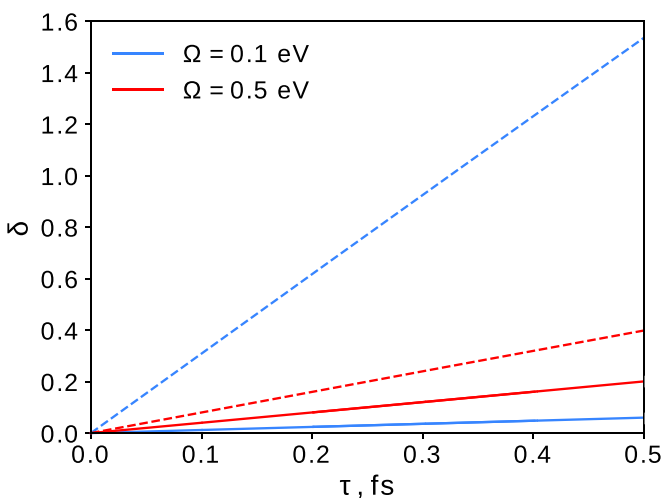


FIG. 6. Comparison of δ computed in full theoretical description in Eq. (15) and analytical approximation in Eq. (11), shown by the solid and dashed lines, respectively. The pulse duration $T = 2$ fs, and two values of $\Omega = 0.1$ and 0.5 eV are shown by the blue (grey) and red (black) lines, respectively.

and δ tends to zero with increasing pulse duration (see Fig. 7). The dependence is more pronounced for the Gaussian pulse shape and for smaller detuning from resonance. For rectangular pulse shapes and $\Omega = 0.5$ eV, the dependence $\delta(T)$ shows the second peak near $T = 5$ fs, otherwise showing nearly linear dependence. The second peak is explained by the fact that the Fourier transform of a non-Gaussian pulse envelope contains, besides the main peak, other spectral harmonics [see side features in the spectra of Figs. 2(b) and 2(d)], whose temporal interaction with the system differs from the main frequency component. Again, the comparison of Gaussian and rectangular pulse shapes in Figs. 7(a) and 7(b), respectively, suggests that the use of a rectangular pulse is more favorable for the effect observation, since δ has larger absolute values for longer pulse duration T .

It is worthwhile to note that most of the presently operating short-wavelength XFELs generate radiation using the self-amplified spontaneous emission (SASE) process, where the radiation is produced stochastically by the electron bunch shot noise. However, the FLASH soft x-ray free-electron laser in Hamburg used in Ref. [10] operates in a special, so-called low electron bunch, charge mode to generate the shortest possible pulses. The low charge enables a very high bunch compression due to smaller space charge effects. The short electron bunch reduces the number of individual longitudinal modes present in the XFEL pulses [20,21], in the ideal case down to a single mode. This is referred to as single-spike SASE or single-mode SASE operation. Single-spike operation delivers sub-5-fs pulses with a high degree of longitudinal coherence from a SASE source. The same is true for other advanced FEL schemes such as seeded XFELs [22].

Our analysis discussed here shows clearly the presence of an additional dynamic phase shift δ , which is explained by only the dynamic interaction of the two-pulse replicas with a two-level quantum system without involving additional mechanisms related to more complex electronic dynamics. One can think, however, that in the real experimental situation several mechanisms can be involved to form a phase shift for linear spectroscopy on atomic systems. For molecular systems, the situation becomes even more complex since vibrational and rotational dynamics may be expected to give an additional contribution to the fine spectral phase shift.

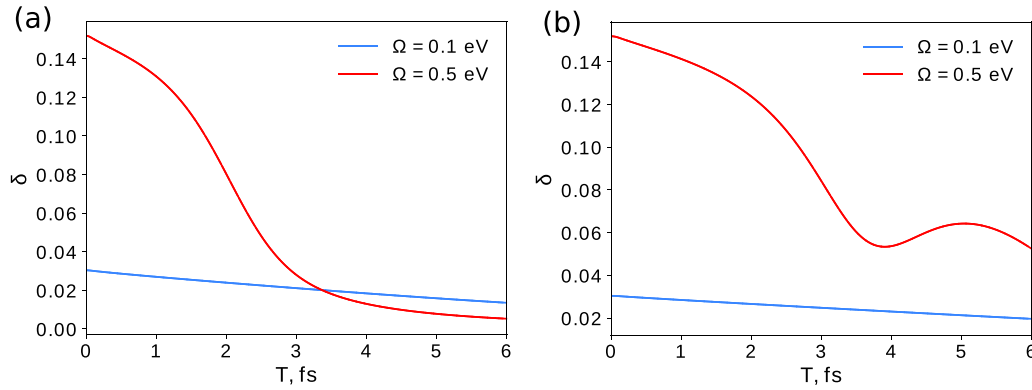


FIG. 7. δ as a function of pulse duration (HWHM) T , for fixed τ and Ω (overlapping pulses). $\tau = 0.2$ fs, $\Omega = 0.1$ and 0.5 eV, (a) $k = 1$, (b) $k = 3$.

IV. SUMMARY

We presented a theory for x-ray absorption and x-ray photoelectron spectra of atoms and molecules interacting with the two coherent and time-delayed x-ray pulses. We have shown that an additional dynamic phase shift is induced in x-ray absorption and have studied its dependence on the pulse parameters. Our theoretical model is based on a general two-level quantum system and thus can be directly applied to a number of systems having electronic transitions in the soft x-ray range, e.g., C K -edge in CO molecules or atomic Ar L -edge. With the help of analytical analysis and numerical simulations we see clearly two distinct phase shifts: (i) a “conventional” phase shift related to the delay time between the coherent pulse replicas, which is equal to $\omega\tau$, and (ii) an additional—dynamic—phase shift δ arising from the interference of the two x-ray pulses with the two-level quantum system. We show strong dependence of the dynamic phase shift value on the x-ray field characteristics such as pulse duration, pulse shape (Gaussian vs rectangular temporal profiles), delay time between the pulses, and energy detuning from resonance with the electronic transition. The dynamic phase shift is absent for on-resonance excitation of the quantum transition and reaches a sharp maximum at particular detuning, the value of which is dependent on the duration of the x-ray pulses. It is shown that the dynamical phase shift is absent in the case of x-ray ionization in full agreement with the experiment [10].

We concluded that the use of rectangular pulses is more favorable for observing the effect as compared to applying Gaussian pulse profiles; the absolute value of δ becomes larger with increasing the delay time between the two x-ray pulses and becomes observable at delay times on the order of the pulse duration $\tau \sim T$. One can expect similar effects in resonant Auger scattering, resonant inelastic x-ray scattering (RIXS), and stimulated RIXS. However, the actual dependencies of the dynamical phase shift in these processes will be different as compared to XAS and XPS, due to different dynamical interference in these scattering processes. The dynamic phase shift is also expected in molecular systems where it may have additional complexity due to the rotational and vibrational dynamics.

ACKNOWLEDGMENTS

The reported study was funded by Russian Foundation for Basic Research (RFBR), Project No. 19-29-12015. F.G. acknowledges also the support from the Helmholtz Virtual Institute VI419 Dynamic Pathways in Multidimensional Landscapes. T.L. acknowledges support by the Deutsche Forschungsgemeinschaft through the Cluster of Excellence “Advanced Imaging of Matter” (EXC 2056 - Project No. 390715994). V.K. acknowledges support from the Vetenskaprådet (Grant No. 2019-03470).

-
- [1] N. B. Baranova, I. M. Beterov, B. Ya. Zel’dovich, I. I. Ryabtsev, A. N. Chudinov, and A. A. Shul’ginov, Observation of an interference of one- and two-photon ionization of the sodium $4s$ state, *JETP Lett.* **55**, 439 (1992).
- [2] Y.-Y. Yin, C. Chen, D. S. Elliott, and A. V. Smith, Asymmetric Photoelectron Angular Distributions from Interfering Photoionization Processes, *Phys. Rev. Lett.* **69**, 2353 (1992).
- [3] V. Wanie, H. Ibrahim, S. Beaulieu, N. Thiré, B. E. Schmidt, Y. Deng, A. S. Alnaser, I. V. Litvinyuk, X.-M. Tong, and F. Légaré, Coherent control of D_2/H_2 dissociative ionization by a mid-infrared two-color laser field, *J. Phys. B: At. Mol. Opt. Phys.* **49**, 025601 (2016).
- [4] M. O. Scully and M. S. Zubairy, *Quantum Optics* (Cambridge University, Cambridge, England, 2001).
- [5] V. Kimberg, F. F. Guimarães, V. C. Felicíssimo, and F. Gel’mukhanov, Phase-sensitive wave-packet dynamics caused by a breakdown of the rotating-wave approximation, *Phys. Rev. A* **73**, 023409 (2006).
- [6] F. F. Guimarães, V. Kimberg, V. C. Felicíssimo, F. Gel’mukhanov, A. Cesar, and H. Ågren, Infrared-x-ray pump-probe spectroscopy of the NO molecule, *Phys. Rev. A* **72**, 012714 (2005).
- [7] Y. Hikosaka, T. Kaneyasu, M. Fujimoto, H. Iwayama, and M. Katoh, Coherent control in the extreme ultraviolet and attosec-

- ond regime by synchrotron radiation, *Nat. Commun.* **10**, 4988 (2019).
- [8] K. C. Prince, E. Allaria, C. Callegari, R. Cucini, G. De Ninno, S. Di Mitri, B. Diviacco, E. Ferrari, P. Finetti, D. Gauthier, L. Giannessi, N. Mahne, G. Penco, O. Plekan, L. Raimondi, P. Rebernik, E. Roussel, C. Svetina, M. Trovó, M. Zangrando, M. Negro *et al.*, Coherent control with a short-wavelength free electron laser, *Nat. Photonics* **10**, 176 (2016).
- [9] L. Giannessi, E. Allaria, K. C. Prince, C. Callegari, G. Sansone, K. Ueda, T. Morishita, C. N. Liu, A. N. Grum-Grzhimailo, E. V. Gryzlova, N. Douguet, and K. Bartschat, Coherent control schemes for the photoionization of neon and helium in the extreme ultraviolet spectral region, *Sci. Rep.* **8**, 7774 (2018).
- [10] S. Usenko, D. Schwickert, A. Przystawik, K. Baev, I. Baev, M. Braune, L. Bocklage, M. K. Czwalinna, S. Deinert, S. Düsterer, A. Hans, G. Hartmann, C. Haunhorst, M. Kuhlmann, S. Palutke, R. Röhlberger, J. Rösch-Schulenburg, P. Schmidt, S. Skruszewicz, S. Toleikis, J. Viehhaus *et al.*, Auger electron wave packet interferometry on extreme timescales with coherent soft x-rays, *J. Phys. B: At. Mol. Opt. Phys.* **53**, 244008 (2020).
- [11] A. Wituschek, L. Bruder, E. Allaria, U. Bangert, M. Binz, R. Borghes, C. Callegari, G. Cerullo, P. Cinquegrana, L. Giannessi, and M. Danailov, Tracking attosecond electronic coherences using phase-manipulated extreme ultraviolet pulses, *Nat. Commun.* **11**, 883 (2020).
- [12] C. Callegari, A. N. Grum-Grzhimailo, K. L. Ishikawa, K. C. Prince, G. Sansone, and K. Ueda, Atomic, molecular and optical physics applications of longitudinally coherent and narrow bandwidth Free-Electron Lasers, *Phys. Rep.* **904**, 1 (2021).
- [13] L. Young, K. Ueda, M. Gühr, P. H. Bucksbaum, M. Simon, S. Mukamel, N. Rohringer, K. C. Prince, C. Masciovecchio, M. Meyer, A. Rudenko, D. Rolles, C. Bostedt, M. Fuchs, D. A. Reis, R. Santra, H. Kapteyn, M. Murnane, H. Ibrahim, F. Légaré, M. Vrakking *et al.*, Roadmap of ultrafast x-ray atomic and molecular physics, *J. Phys. B: At., Mol. Opt. Phys.* **51**, 032003 (2018).
- [14] F. Gel'mukhanov, M. Odelius, S. Polyutov, A. Föhlisch, and V. Kimberg, Dynamics of resonant x-ray and Auger scattering, *Rev. Mod. Phys.* **93**, 035001 (2021).
- [15] S. Hüfner, *Photoelectron Spectroscopy, Principles and Applications* (Springer-Verlag, Berlin, 2003).
- [16] Y.-P. Sun, J.-C. Liu, C.-K. Wang, and F. Gel'mukhanov, Propagation of a strong x-ray pulse: Pulse compression, stimulated Raman scattering, amplified spontaneous emission, lasing without inversion, and four-wave mixing, *Phys. Rev. A* **81**, 013812 (2010).
- [17] P. Skytt, P. Glans, K. Gunnelin, J. Guo, and J. Nordgren, Lifetime-vibrational interference effects in the resonantly excited x-ray-emission spectra of CO, *Phys. Rev. A* **55**, 146 (1997).
- [18] S. Usenko, A. Przystawik, M. A. Jakob, L. L. Lazzarino, G. Brenner, S. Toleikis, C. Haunhorst, D. Kip, and T. Laarmann, Attosecond interferometry with self-amplified spontaneous emission of a free-electron laser, *Nat. Commun.* **8**, 15626 (2017).
- [19] S. Usenko, A. Przystawik, L. L. Lazzarino, M. A. Jakob, F. Jacobs, C. Becker, C. Haunhorst, D. Kip, and T. Laarmann, Split-and-delay unit for FEL interferometry in the XUV spectral range, *Appl. Sci.* **7**, 544 (2017).
- [20] R. Bonifacio, L. DeSalvo, P. Pierini, N. Piovella, and C. Pellegrini, Spectrum, Temporal Structure, and Fluctuations in a High-Gain Free-Electron Laser Starting from Noise, *Phys. Rev. Lett.* **73**, 70 (1994).
- [21] E. L. Saldin, E. A. Schneidmiller, and M. V. Yurkov, *The Physics of Free-Electron Lasers* (Springer-Verlag, Berlin, 1999).
- [22] O. Y. Gorobtsov *et al.*, Seeded X-ray free-electron laser generating radiation with laser statistical properties, *Nat. Commun.* **9**, 4498 (2018).